VISUALIZING THE EVOLUTION OF CHARGE DENSITY IN FULVENE BOND TORSION: A BOND BUNDLE CASE STUDY

by

Jordan Goss

A thesis submitted to the Faculty and the Board of Trustees of Colorado School of Mines in partial fulfillment of the requirements of the degree of Master of Science (Applied Chemistry).

Golden, Colorado

Date _____

Signed: _____
Jordan Goss

Signed: _____
Dr. Mark E. Eberhart
Thesis Advisor

Golden, Colorado

Date _____

Signed: _____
Dr. Tom Gennett
Professor and Head
Department of Chemistry and Geochemistry

ABSTRACT

The chemical bond is a central concept of many sciences, but there is no unified consensus as to the physical representation of a bond, or how this representation relates to a bond's properties. A variety of bonding models have been proposed, each different in its explanation and prediction of chemical properties. Quantum theory of atoms in molecules (QTAIM) aims to encompass a well-rounded approach applicable to many areas of molecular studies. The QTAIM bonding model uses the topology of the electron charge density ($\rho(r)$) and defines bonding interactions as one-dimensional ridges of $\rho(r)$—known as bond paths. As with any bonding model, there are instances where its predictions do not provide a full picture. For example, a 1D bond path does not accurately describe properties of interest, such as an accounting of the energy barrier to bond torsion.

A bond bundle analysis case study presented in this thesis analyzes the π-bond rotation in a computational benchmark molecule, fulvene. This methodology is an extension of QTAIM and illustrates the applicability of charge density based methods to bonding. We demonstrate the bond bundle can capture the same type of chemical information as valence bond or molecular orbital theories. The bond bundle accurately represents the transition from double to single bond character in fulvene by qualitative and quantitative observation of the evolution in size and shape of the bond bundle.

ACKNOWLEDGEMENTS

I would like to gratefully acknowledge the funding sources necessary for the completion of this work including the Colorado School of Mines Department of Chemistry and Geochemistry for my teacher assistantships and the Office of Naval Research (Grant No. N00014-10-1-0838).

I would also like to acknowledge my advisor and mentor Dr Mark E. Eberhart, and the input and guidance from my thesis committee members: Dr. Shubham Vyas and Dr. Allison Caster. I would like to give a special thank you to my group members for their support and guidance: Dr. Travis Jones, Dr. Amanda Morgenstern, Dr. Jonathan Miorelli, Tim Wilson, and Malavikha Rajivmoorthy.

Lastly, I would like to give a warm thank you to my family for their support, patience, guidance, and love during my Master's thesis: Alex Gribben, Jack and Melanie Goss, Paige and Elizabeth Goss, Blair Goss, Shelby Goss, and Aurora Christiansen.

TABLE OF CONTENTS

LIST OF FIGURES

LIST OF TABLES

LIST OF SYMBOLS

Atomic Basin . . . . . Ω

Charge density at a bond critical point . . . . . ρ_b

Curvature of charge density in principle direction i . . . . . λ_1

Diagonalized Hessian . . . . . Λ

Electron charge density . . . . . $\rho(r)$

Electron count . . . . . N

Ellipticity . . . . . ε

Gradient kinetic energy . . . . . G

Gradient of charge density . . . . . $\nabla\rho$

Hessian of the charge density. . . . . H(ρ)

Laplacian . . . . . $\nabla^2\rho(r)$

Mononuclear region . . . . . $\partial\Omega$

Normal vector. . . . . n(r)

Nuclear coordinates . . . . . X_A

Schrödingier kinetic energy . . . . . K

Total energy . . . . . E

Total kinetic energy . . . . . T

Total potential energy. V

Wave function . . . . . $\psi(r)$

Work of separation . . . . . W_∞

LIST OF ABBREVIATIONS

Amsterdam density functional package . . . . . ADF

Atom in a molecule . . . . . AIM

Bond bundle . . . . . .BB

Bond critical point . . . . . bCP

Bond order . . . . . .BO

Complete active space self-consistent field . . . . . .CASSCF

Correlation-consistent polarized valence double-zeta basis set . . . . . .cc-pVDZ

Coulomb-attenuating-method-Y-Becke-3-Lee-Yang-Parr CAMY-B3LYP

Critical point . . . . . CP

Degrees of freedom . . . . . .DOF

Density functional theory . . . . . DFT

Electron preceding perspective . . . . . EPP

Gradient bundle analysis. . . . . GBA

Gradient path. . . . . .GP

Kinetic energy . . . . . KE

Nuclear CP . . . . . .nCP

Quantum theory of atoms in molecules . . . . . .QTAIM

Relative critical set . . . . . RCS

Spin orbital . . . . . .SO

Spin restricted . . . . . SR

Spin unrestricted . . . . . SU

Zero-flux surface . . . . . ZFS

CHAPTER 1

INTRODUCTION- TOPOLOGICAL CHEMICAL BONDING MODEL

The advancement of chemical bonding models is important to the progress of chemistry by creating better understanding and control of interactions between atoms. Lewis, London, and Heitler provided various representations for the chemical bond and bonding nearly a century ago. Pauling, Mulliken, and Slater refined these models in the 1930's and these refinements represent the foundations of our current bonding models. QTAIM (1) and conceptual density functional theory (2) are more recent additions to the menagerie of bonding models but are not widely used by researchers or extensively discussed in chemistry texts. These newer bonding models help scientists transform the process of designing new molecules and materials by changing the perception and assessment of atomic interactions.

The case study present in this thesis uses the bond bundle to visualize and analyze bond torsion. Through this case study I aim to provide additional applications to the QTAIM based approaches, and provide a fuller picture of bonding interactions. Here I will review my work and that of my fellow researchers in the Molecular Theory Group, which demonstrates that QTAIM formalisms extend our understanding of rotation about a π-bond. Specifically, the bond bundle is used as a qualitative and quantitative technique to capture bonding interactions, like bond order, during bond torsion. From this case study I will extend our understanding of bond torsion to the barrier of rotation in different molecules. From this study, changes in the charge density caused by bond torsion can directly be related to increasing or decreasing energy barriers to rotation.

1.1. Quantum Theory of Atoms in Molecules

QTAIM uses the topology of the charge density (ρ(r)) to define atomic properties and analyze bonding interactions. In particular, QTAIM has helped to deepen our understanding of

chemical bonding, atomic interactions, as well as the strength and stability of molecules. Richard Bader developed QTAIM in the 1970's. He was motivated to discover if it was possible to delineate the boundaries of an atom in a molecule and if bonds can be observed (1,3).

The electron charge density is an observable feature, unlike the complex valued wave function, $\psi(r)$. The wave function gives great insight into chemical interactions, but is not a quantum-mechanical observable. The charge density is a measurable feature and always real valued functions. Advancements with x-ray crystallography enable scientists to measure the charge density experimentally. Bader and others have argued that a bonding model must be based off something real (4,5), which provided the motivation for QTAIM. The original theory gives insight into chemical interactions through two topological features: bond critical points (and corresponding bond paths) and atomic basins.

1.1.1. Critical Points

QTAIM has proven useful as a way to associate molecular and solid state properties with the structure of $\rho(r)$, where structure is characterized in terms of topological and geometric properties (1,6–8). In turn, and quite generally, the topology of $\rho(r)$ can be categorized by way of the elements of its relative critical sets (RCSs), which are defined according to the orthogonality between the three eigenvectors (ε_i, $i \in \{1, 2, 3\}$) of the Hessian of charge density ($H\rho$) and its gradient ($\nabla\rho$) (9).

Elements of the 0-, 1-, and 2-dimensional RCSs are respectively the sets of points where three, two, or one of the eigenvalues of $H\rho$ are orthogonal to $\nabla\rho$, i.e., where

$$\nabla\rho(r)\cdot\varepsilon_i = 0. \tag{1.1}$$

Elements of the 0-D RCS are the points where ∇ρ vanishes, and as such, are the critical points (CPs) of Morse Theory—maxima, minima, and saddle points of index +1 and -1 (10). Elements of the 1-D RCS are special gradient paths (GPs), which must originate and terminate at CPs. Elements of the 2-D RCS are special gradient surfaces that are necessarily bounded by elements of the 1-D RCS. QTAIM formalism (1) associates chemical structure with elements of the RCS. For example, charge density maxima are coincident with nuclei and hence are called nuclear-CPs (nCP). An element of the 1-D critical set connecting two nCPs is called a bond path and must pass through a -1 saddle point called a bond-CP (bCP). An example of CPs and bond paths is highlighted in Figure 1.1.

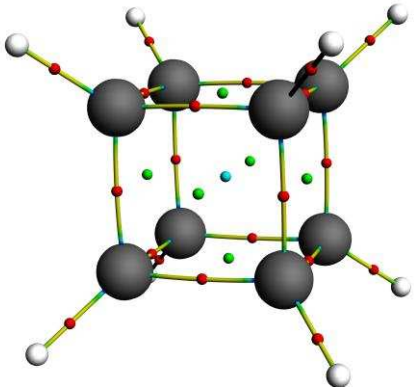

Figure 1.1: The CPs and bond paths in a cubane molecule. The image has CPs labeled as follows: C-grey, H-white, bond CPs-red, ring CPs-green, and cage CPs-blue. CPs and bond paths were calculated using Amsterdam Density Functional (ADF) package (11,12).

The geometry of the charge density at critical points provides additional information about bonding character. Bond order and corresponding bond strength has been correlated with the amount of charge density at a bond CP (1) through the relationship,

$$BO = e^{A(\rho_b - B)} \tag{1.2}$$

where A and B are constants dependent on the bond and ρ_b is the value of charge density at the bond CP. Correlation between bond strength and electron charge density at bond CP has proven useful in characterizing hydrogen bonds (13).

Bader argued the curvature at a critical point can indicate type of bonding interaction (1). The Hessian of the charge density determines the curvature at critical points.

$$\Lambda = \begin{bmatrix} \frac{\partial^2 \rho}{\partial x^2} & 0 & 0 \\ 0 & \frac{\partial^2 \rho}{\partial y^2} & 0 \\ 0 & 0 & \frac{\partial^2 \rho}{\partial z^2} \end{bmatrix} = \begin{bmatrix} \lambda_1 & 0 & 0 \\ 0 & \lambda_2 & 0 \\ 0 & 0 & \lambda_3 \end{bmatrix} \tag{1.3}$$

The lambda values ($\lambda_1, \lambda_2, \lambda_3,$) are curvatures of the charge density in three principle directions. For example, at a bond CP, one eigenvector of the Hessian is parallel to the bond path and always positive (λ_3), while the other two are perpendicular to the bond path and negative (λ_1 and λ_2). The Laplacian, the trace of the Hessian, further characterizes bonding interactions. A positive Laplacian value occurs when curvature along the bond path is greater than the sum of curvatures perpendicular to the bond path, meaning charge density depletion around bond path. Bader argued a positive Laplacian indicates closed-shell bonding interactions such as ionic or Van der Waals bonding (1). A negative Laplacian value associated with open-shell interactions, or covalent bond, results in concentration of charge density at bond CP (14).

The Hessian of the charge density can further define changes that occur within the charge density. The ellipticity is defined using the two negative values of λ at a bond CP

$$\epsilon = \frac{\lambda_1}{\lambda_2} - 1 \tag{1.4}$$

where $|\lambda_1| > |\lambda_2|$. An ellipticity value near zero indicates cylindrical distribution of density around a bond path indicative of a single or a triple bond. A maximum ellipticity value shows unequal density distribution and therefore indicates a π-bond. Jenkins *et al.* used ellipticity to study water clusters, and found a correlation between high ellipticity and higher energy water clusters (15). From this, Jenkins concluded the most stable water clusters were those with least number of hydrogen bonding interactions.

In summary, the values of the charge density, Hessian (ellipticity), and Laplacian at a bCP are used to classify and understand bonding interactions. They are used to show how properties at a bCP can correlate with bond strength and stability. These values can be determined experimentally or theoretically because they are based on the real value charge density and not the complex value wave function. Over all, QTAIM provides an intuitive way to assess thermodynamic properties, stability of molecules, and selectivity of reaction pathways.

1.1.2. Bond Paths

Bond paths are defined as the union between the two gradient paths in ρ(r) originating at a bond CP and terminating at nuclear CPs (16). A 1D bond path increases the chemical information gained compared to 0D CPs. In highly symmetric systems and linear systems bond paths lie along the internuclear axis. In some cases, bond paths that deviate from this axis correlate to the stability of bonding interactions. For example, ring structures like that of cyclic propane (Figure 1.2) have outward curved bond paths indicative of ring strain. On the other hand, bond paths that curve inward toward the ring center, for instance in benzene, have been argued to be indicative of ring stability.

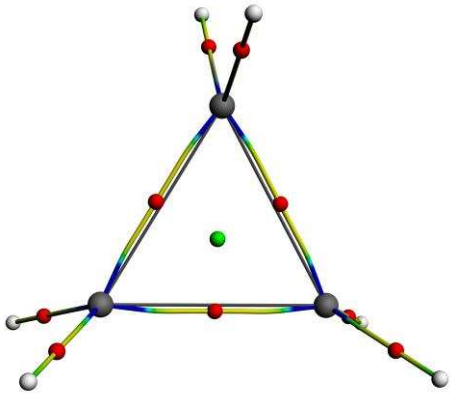

Figure 1.2: Bond paths (colored) and internuclear axes (grey) in cyclopropane. The outward curved bond paths, compared to the internuclear axis, between the carbon atoms indicate ring strain in the molecule (12).

Arguments have been made that a bond path is not always symbolic of a stabilizing bonding interaction. Some systems have been found where the bond path connecting two nuclei are repulsive in nature. The disagreement concerning the interactions involving a bond path indicates a need for further development of the current bonding model.

1.1.3 Atomic Basins and Zero Flux Surfaces

In addition to 1D lines, QTAIM defines physical boundaries for 3D quantum atoms within molecules (1). An atom in a molecule (AIM), referred to as a Bader atom or atomic basin, can be found by following a collection of gradient paths to a nuclear CP. All gradient paths that terminate at a nuclear CP cover the space defined as an atomic volume. Atomic basins are bounded by surfaces of zero flux in $\nabla\rho(r)$ meaning no gradient path can cross these surfaces and the zero-flux surface (ZFS) condition is satisfied by

$$\nabla\rho\,(r)\cdot n(r) = 0, for\ all\ r\ \in\ \partial\Omega \tag{1.5}$$

where $\partial\Omega$ is the boundary of mononuclear region and n(r) is a normal vector (see Figure 1.3 for a visual representation of an atomic basin).

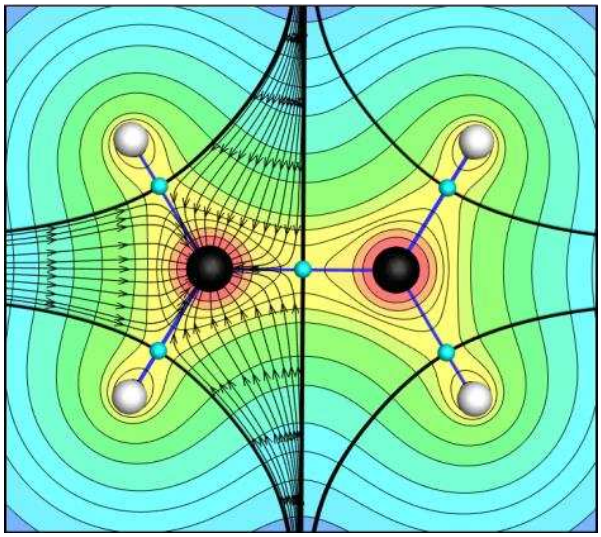

Figure 1.3: 2D cut plane of the charge density of ethene in the plane of the molecule. The thick black lines represent the ZFS containing the carbon (black) atomic basins. Thin black lines within the atomic basins show all the gradient paths within the atomic basin.

Atomic basins have well-defined properties, such as energy, due to the zero-flux surface condition. An arbitrary volume in the charge density does not have a well-defined kinetic energy because local kinetic energy at any point is ambiguous (17,18). Total kinetic energy can be calculated by integration of the Schrodinger kinetic energy,

$$K(\Omega) = -\frac{\hbar^2}{2m} N \int_{\Omega} dr \int d\tau' (\psi \nabla^2 \psi^* + \psi^* \nabla^2 \psi) \tag{1.6}$$

or the gradient kinetic energy,

$$G(\Omega) = -\frac{\hbar^2}{2m} N \int_{\Omega} dr \int d\tau' \nabla_i \psi^* \cdot \nabla_i \psi \tag{1.7}$$

or through linear combination of these two equations (17). In order for kinetic energy to be well defined, the Schrödinger kinetic energy must be equal to the gradient kinetic energy. These two equations differ only by a term proportional to the Laplacian.

$$K(r) = G(r) - \frac{\hbar^2}{4m} \nabla^2 \rho(r) \tag{1.8}$$

Integration over the above equations allows one to compute the difference in the average kinetic energy in a volume, Ω. Using Gauss's theorem, the difference can be written in terms of a surface integral,

$$K(\Omega) = G(\Omega) - \frac{\hbar^2}{4m} N \int dS(\Omega, r) \nabla\rho(r) \cdot n(r) \tag{1.9}$$

which will be zero for any volume bounded by a zero-flux surface in the gradient of charge density. Hence, any volume bounded by a zero-flux surface has a well-defined kinetic energy, and therefore total energy, and properties dependent on the energy. This partitioning of space gives additive properties of atoms within molecules. One can find the charge, energy, and volume, to name a few, by integrating over all atomic basins.

Bader also demonstrated that the virial theorem is satisfied over any region bounded by a zero-flux surface. The virial theorem gives the total energy of a system based on the kinetic energy. The total energy can be written is terms of density functional theory (DFT) as (19)

$$E = -T(\rho) - \sum_A X_A \frac{\partial E}{\partial X_A} \tag{1.10}$$

where T is the total kinetic energy functional and X_A are the nuclear coordinates. The total energy can also be found by using the kinetic energy (T) and potential energy (V) functionals.

$$E = T(\rho) + V(\rho) \tag{1.11}$$

At any stationary point, the potential energy term goes to zero and the total energy can be calculated as

$$E = -T(\rho). \tag{1.12}$$

As a result, regions over which the kinetic energy is well-defined, the total energy of a volume in (ρ) can be calculated.

1.2 Bond Bundles

Atomic basins are the only volumes recognized by the original QTAIM; however, they are not the only volumes in the charge density bounded by ZFSs containing well-defined properties. Pendás defined a primary bundle as set of gradient paths that start at a minimum and end at a maximum in ρ(r) (20). These bundles are bounded by ZFSs and have only one nuclear CP, one cage CP, n ring CP, and n bond CP on the surface of each bundle (20). The union of these primary bundles sharing a nCP creates an atomic basin of attraction defined by Bader (1). Pendás defined primary bundles that share a single cage point as an atomic basin of repulsion.

Atomic and repulsive basins are bounded by one ZFS making it easy to locate these basins in the charge density. Saddle points in the charge density are bounded by an infinite number of ZFS as shown in Figure 1.4.

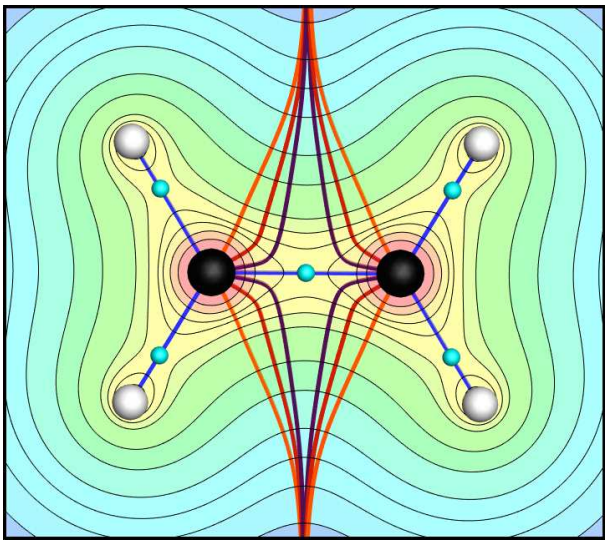

Figure 1.4: 2D cut plane of the charge density of ethene in the plane of the molecule. The thick colored lines show a sampling of ZFSs bounding the C-C bond CP (12).

Eberhart noted some of these ZFSs are special as they are contained within the relative critical set definition of ρ(r) (21). The BB is defined as a volume bounded by ZFSs satisfying the 2D relative critical set definition and containing a single bond CP. The BB has well defined additive

properties just like an atomic basin because of the ZFS condition, and recovers properties consistent with the well-known picture of a bond (22).

Bond bundles are used to uncover structure-property relationships within molecules. BBs have characteristic shapes that have been argued to mediate chemical reactivity (23), and can be described most generally as open or closed. For example, as shown in Figure 1.5, ethane is a closed BB because its faces are asymptotically converging. On the other hand, ethene is open in one direction, with diverging faces perpendicular to the molecular plane, but closed parallel to the plane.

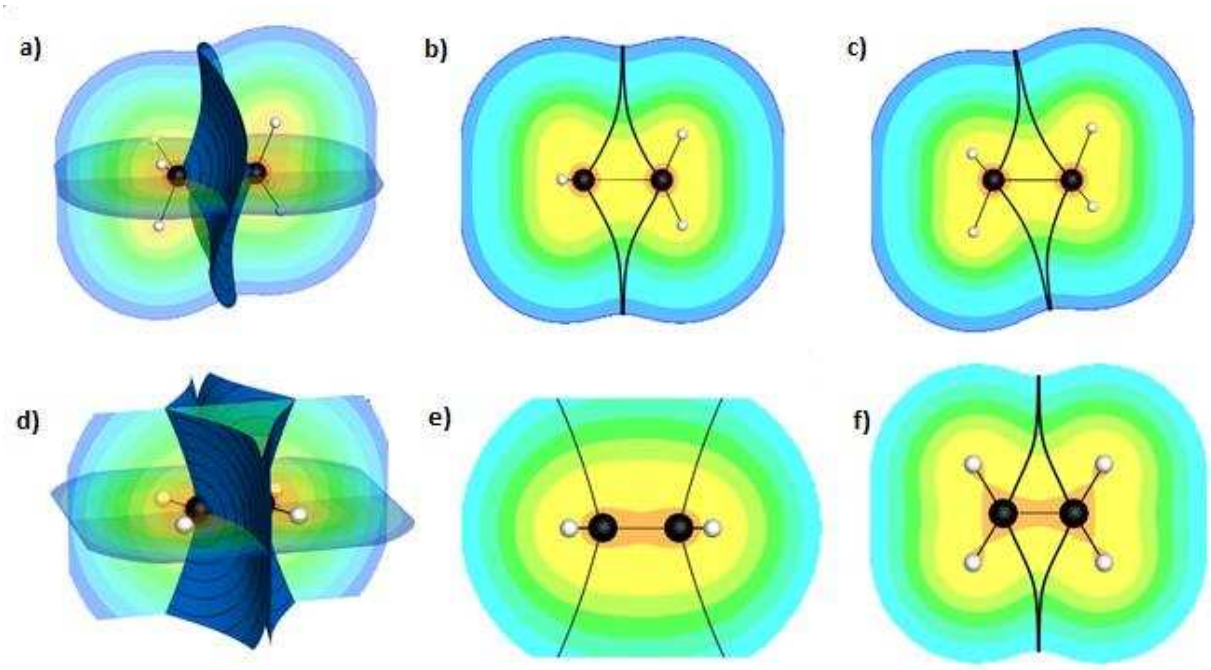

Figure 1.5: (a-c): The surfaces of the C-C bond bundle of ethane and two perpendicular cut planes containing the C-C axis. The intersection of the bond bundle with the xz (b) and yz (c) cut plane. Note the convergence of the bond bundle surfaces in this plane. (d-f): The surfaces of the C-C bond bundle of ethane and two cut planes. The surfaces of this bond bundle are diverging perpendicular to the xz plane shown (e), and converging in the plane of the molecule (f). The bond bundle of ethene is said to be open normal to the molecular plane and closed in the plane.

As volumes, BBs can be used to make contact with the chemical concept of bond order (23) as half the number of valence electrons it contains. BB bond order can be determined using only the total charge density by assuming a radial distribution of core electrons as demonstrated in (6). In practice, this number can equivalently be determined from an electronic structure calculation by integrating the valence electron density of the BB out to an arbitrarily distant cutoff surface, typically chosen as the 0.001 electron/bohr^3 isosurface (1,24). Using this integration scheme, the ethane C-C bond order is 0.91 and the bond order of ethene is 1.72.

Jones showed the shape and size of BBs can be used to predict nucleophilic substitution or addition (6). A BB with a smaller volume directly correlates with less valence electrons. When a bond breaks, the BB must collapse, and therefore, a closed BB is energetically easier to interrupt and will more readily undergo nucleophilic substitution or addition. The BB can also be used to connect electron count and material toughness. The valence electrons in a BB was found to correlate with work of separation (W_∞) in a study finding alloying elements for high strengths steels (25). The valence electrons in a BB of second neighbor iron atoms correlate linearly with W_∞, and tougher materials can be created using various transition metals as alloying elements.

The Bond Bundle Model presents chemical bonds as topological connections between atoms and as regions with well-defined properties. We can now use this model to broaden the way we assess the charge density. The BB adds a layer of investigation into the geometrical connectivity of $\rho(r)$, and not limited solely to the topological features of $\rho(r)$.

CHAPTER 2

VISUALIZING THE EVOLUTION OF CHARGE DENSITY IN FULVENE BOND TORSION: A BOND BUNDLE CASE STUDY

Modified from a manuscript submitted to *Physical Chemistry Chemical Physics*.

Jordan Goss[1], Timothy Wilson[2], Amanda Morgenstern[3], M.E. Eberhart[4]. 2017.

2.1 Abstract

The chemical bond is central to understanding chemical reactivity and has motivated numerous methods to characterize and model its behavior, including particularly molecular orbital approaches. Less used are models based on the electron charge density. To illustrate the ability of charge density based methods, we present a case study of the exo-double bond rotation in a fulvene molecule using bond bundle analysis, which is an extension to the QTAIM. Analysis is performed on both the ground and first excited state where the barrier to rotation involves a conical intersection between the two states. We demonstrate that bond bundles can be used to capture the same chemical information recovered from orbital methods. Most notably, bond bundles are found to accurately represent the transition between single and double bond character stemming from visual observation of the evolution of the size and shape of the bond bundle.

2.2 Introduction

Valence bond and molecular orbital theories are the most common formalisms used to visualize and predict the redistribution of electrons accompanying atomic movement. These

[1] Primary researcher and author
[2] Developed code and provided advice on computations
[3] Performed QTAIM analysis and document editing
[4] Corresponding author

approaches complement one another by providing different vantage points from which to view an inherently complex and only partially understood phenomenon. Similarly, we have found that the less well known approach employing the QTAIM (1) and its recent extensions may further enrich our understanding of electron redistribution and be especially useful for visualization.

The complementary value of QTAIM methodologies is that they are motivated by the desire to associate molecular properties with a physical observable—the topology and geometry of the charge density. As such, these methods are consistent with the foundational principles of density functional theory (DFT), lend themselves to easy visualization, and can be applied to any system in which $\rho(r)$ is known to some arbitrary accuracy, for example as determined via orbital based methods, orbital free approaches, or even experimentally determined densities.

One of the first QTAIM efforts to describe the evolution of $\rho(r)$ accompanying atomic motion originated with Bader's applications of catastrophe theory to elucidate the topological constraints to charge redistribution (1). From this perspective, it is not the movement of individual electrons that is of concern, but rather the movement of charge density critical points (CPs)—maxima, minima, and saddle points.

With CPs replacing electrons as the focus of attention in the QTAIM approach, Ayers *et al*. proposed an electron preceding perspective (EPP) (26) which predicts that CP movement occurs most readily along directions where charge density is flattest. Jenkins *et al*. expanded on the EPP through an investigation of the exemplary fulvene system (27). In particular, Jenkins focused on the changes to and about the CP characteristic of fulvene's exo-double bond as it underwent a 90^{o} rotation—a process accompanied by a conical intersection of its ground and excited state potential energy surfaces. Jenkins *et al*. demonstrated that a rotation about this bond

produced changes to the CP, which from the EPP are consistent with experimental observations (26). They showed that flatter charge densities correlate with increased compliance of $\rho(r)$ and lower barriers to rotation.

An interesting aspect of this work was the assessment of the C-C bond evolution from double to single character as a result of the rotation. This assessment used density related arguments based on the ellipticity of $\rho(r)$ of the CP characteristic of the rotated bond. The authors also introduced a new analysis tool based on a 2-dimensional representation of the charge density using "atomic basin set paths" as a visual indicator of bond stiffness, and in turn, determine single versus double bond character. From these arguments, it was possible to comparisons between the density based description of single and double bond character with the orbital based perspective of π-bond rotation.

Here we expand the QTAIM approach a step further by employing extensions to QTAIM that are able to recover a richer representation of charge density evolution. Building on the work of Jenkins *et al*., we demonstrate that these extensions illuminate the behavior of electrons during bond rotation both quantitatively and through an intuitive 3-D visualization.

2.3. Experimental Methods

Our objective for this investigation was to assess BB utility by following the evolution of the charge density of a fulvene molecule accompanying rotation around its exo-double bond (Figure 2.1). As mentioned, our choice of this system was prompted by the study of Jenkins *et al*., who, working at the CASSFC/cc-pvdz level of theory with an active space of six electrons in six orbitals (27–30), identified atomic coordinates for structures on the ground state potential energy surface for rotations of 0^o, 63^o and 90^o degrees, which we refer to respectively as S_0, S_{63}

and S_{90} (Coordinates in Tables A.1-A.3). More interesting, however, was finding that S_{63} and S_{90} lie along the seam of a conical intersection between the ground and excited state.

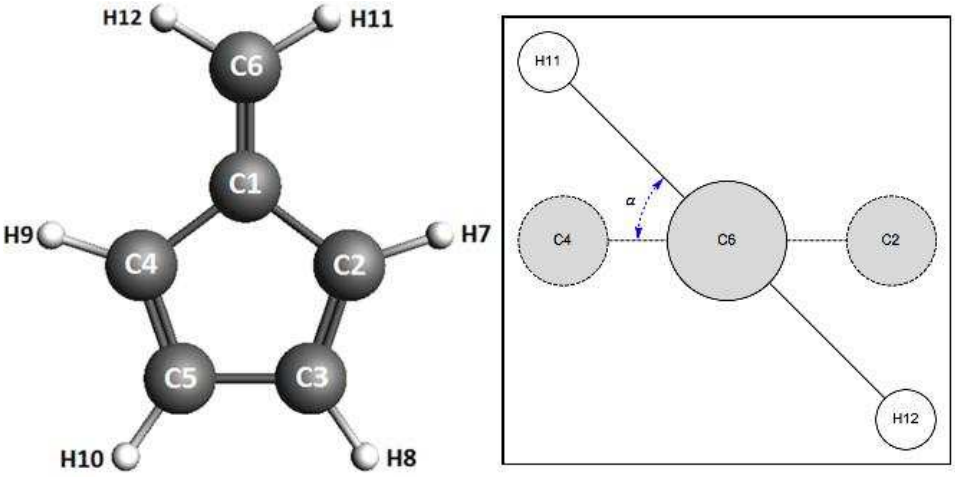

Figure 2.1: Fulvene molecule (left) with carbon (C1-C6) and hydrogen (H7-H12) atoms labeled. The rotation of the methyl group about the C1-C6 bond axis is depicted on the right. The methyl group is rotated in 10 degree increments from planar to the ring (0 degrees) to perpendicular to the ring (90 degrees).

We used molecular-orbital DFT methods to calculate the electronic structure and charge density of the fulvene molecule at nine roughly 10^{o} rotational increments about the C1-C6 bond. Molecular coordinates along the rotation were determined by treating the steps between 0° and less than 63^{o} as rigid rotations of the methylene group of S_0 and those between 63^{o} and less than 90^{o} as ridged rotations of S_{63}. At each point of the rotation the total energies, spin orbital (SO) energies, and charge densities were obtained with the Amsterdam Density Functional Package, ADF, version 2016 (11), employing an all-electron relativistic triple ζ singly polarized basis set and the CAMY-B3LYP functional (31). This functional is a range separated hybrid and recovers quality information for the frontier orbitals essential for excited state calculations. In addition, these same elements of the electronic structure were determined at selected geometries for the first excited state, and at various points an analysis was conducted to determine the sensitivity of

BB parameters to small changes in nuclear coordinates (see Table A.4 and Table A.5). Values of the charge density were imported into Tecplot on a 0.049 grid size. The Bondalyzer add-on package in Tecplot was used to analyze the BBs and valence electron count (32).

The ground state of S_0 was found to have an occupancy for the near Fermi energy orbitals of $\{12A^2\ 9B^2\ 10B^0\}$ which we refer to as the SR-state (spin restricted). The occupancy of the near Fermi energy orbitals for the first excited state of S_0 was found to be $\{12A^2\ 9B^1\ 10B^1\}$, referred to as the SU state (spin unrestricted). To see a physical representation of the SO levels see Figure 2.2. The SU state admits both a singlet and triplet configuration. Throughout our calculations, however, the triplet configuration was of slightly lower energy (~ 0.1 eV). Further, the SOs, and density for the two states were inconsequentially different. Hence all reference to the SU state indicates the triplet configuration.

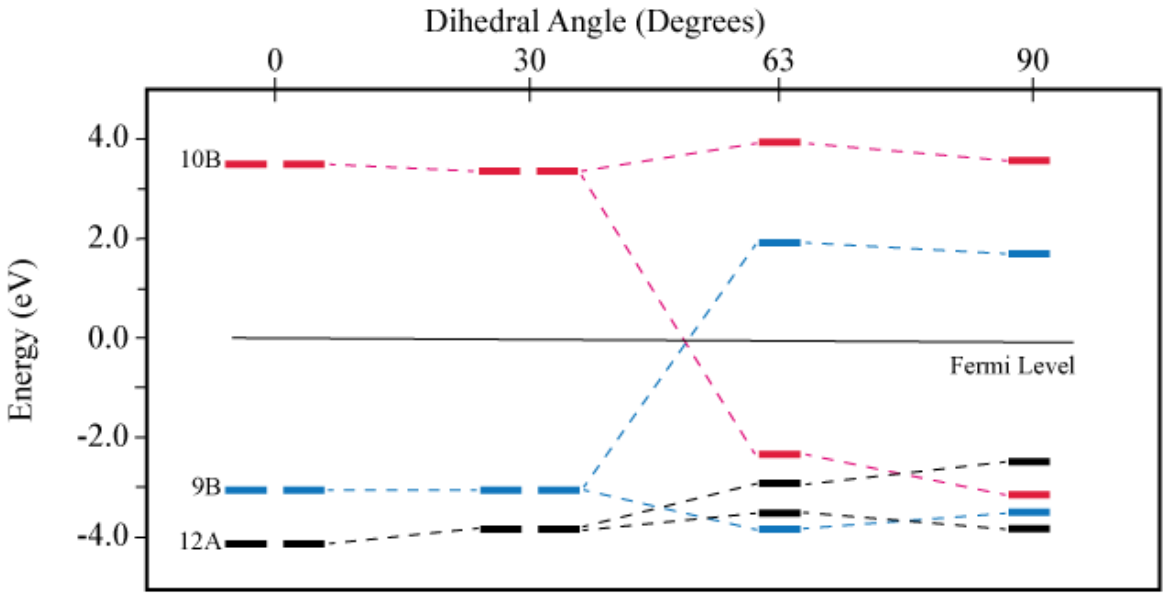

Figure 2.2: The SO levels diagram for the 0 and 30 degree SR (spin restricted), and 63 and 90 degree SU (spin unrestricted) geometries are shown. The most stable state of S_0 has a full occupancy for the near Fermi energy orbitals.

2.4. Results and Discussion

BBs at selected points for both the SR and SU states are shown in Figure 2.3. The BB of planar fulvene is open, resembling the C-C BB of ethene and has a bond order of 1.66 SR and 1.71 SU. Upon bond rotation, the BB begins to close (Figure 2.3) and the bond order decreases (Figure 2.4). The SU BB closes more rapidly than the SR, which is consistent with Hammond's Postulate, i.e. the BB at the transition state resembles that of the SU state and so lies close in energy. The orbital crossing (Figure 2.2) near S_{63} is indicative of a conical intersection. At and near this point, the Born-Oppenheimer approximation is not strictly valid and there may be vibronic contributions that makes separation of electronic and nuclear DOF questionable (33), nonetheless, at 63^{o} degrees the SR and SU bond orders are 1.18 and 1.55 respectively.

Beyond 63^{o}, the responses of the SR and SU BBs to further rotation change. For the SR, though the BB continues to close, the bond order increases. On the other hand, the bond order of the SU decreases as expected. At full rotation, both the SR and SU BBs are fully closed, (all surfaces are asymptotically converging) and resemble the single bond of ethane, with bond orders of 1.97 and 1.24 respectively. Plotting the BB valence electron count (Figure 2.4) throughout the rotation reveals a nearly monotonically decreasing function for those states where the SO occupancy obeys Fermi statistics. The valence electron count achieves its minimum value at S_{90} with bond order equal to 1.24 or equivalently 2.48 valence electrons in the C-C BB. (For a table of many calculated parameters of the fulvene rotation see Table A.6.)

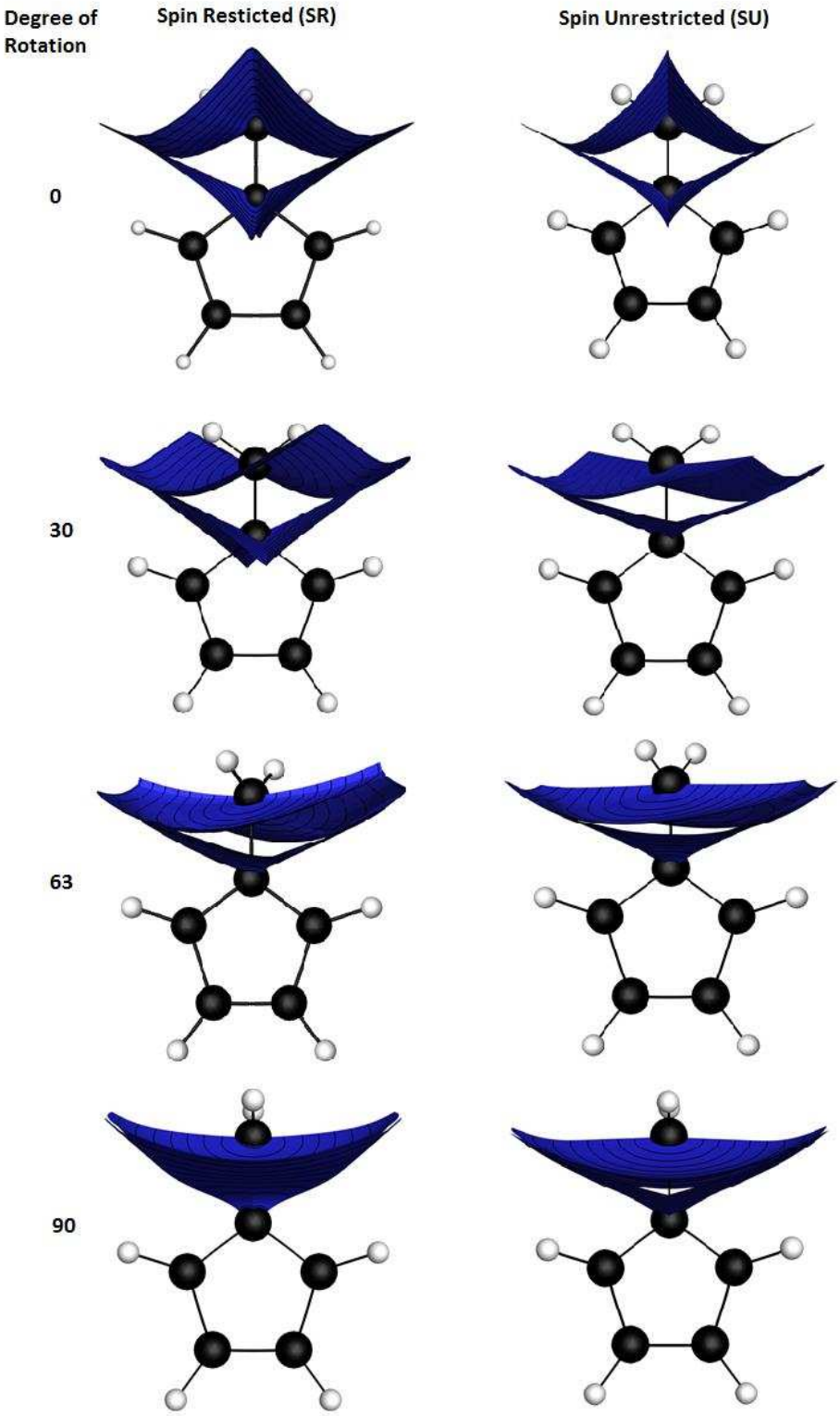

Figure 2.3: Fulvene C1-C6 bond bundles for the SR and SU states as a function of rotation angle.

Throughout the rotation, the C-C bond loses 0.94 electrons. At the same time, the number of electrons in the two C6-H bonds increases by 0.32 electrons. The remaining 0.62 electrons are now distributed across the C ring. Bader analysis of spin densities is consistent with our BB analysis, showing excess spin up electrons located on C6 and the ring (see Table A.7).

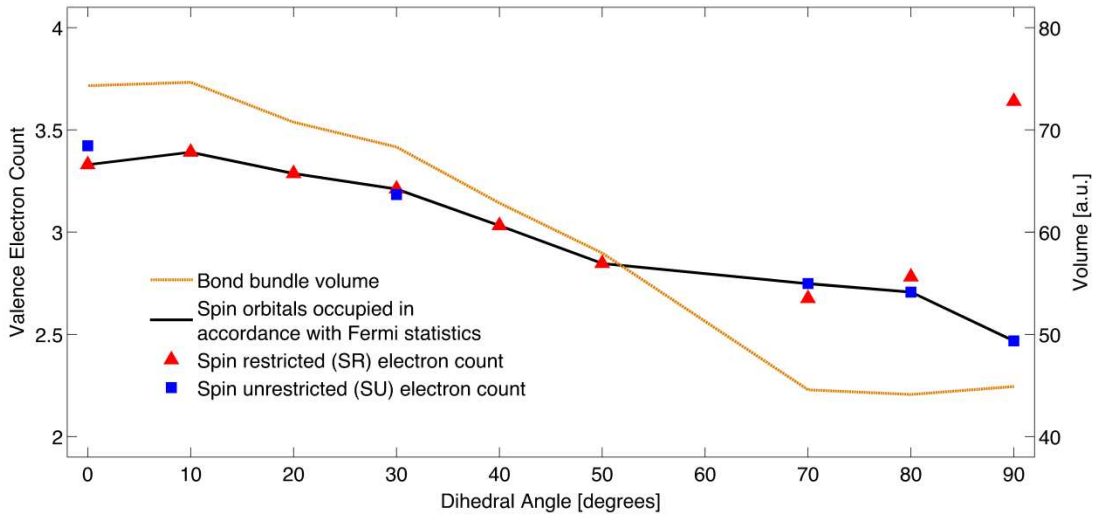

Figure 2.4: The valence electron count and volume in the C1-C6 bond bundle for the full rotation of the methylene group on fulvene. The SR state (triangles) shows a generally decreasing electron count from 0 to 63 degrees. The SU state (squares) initially shows consistent electron counts with the ground state, however beyond 63° the electron count within the bond bundle continues to decrease for the SU state, but increases for the SR state. The black line connects the states with SOs occupied in accordance with Fermi statistics.

The conventional view of the breaking of a C-C double bond is the result of the occupancy of a π antibonding orbital with a corresponding change in bond order of 1. However, such a view is a convenience only, and strictly applicable to a diatomic system where there is but one pair of bound atoms. Figure 2.5 depicts the 12A and 10B SOs coupled by the bond rotation, with the resulting occupation of the 10B SO beyond a 63° rotation. While this SO may be described as anti-bonding between C1 and C6, it is simultaneously bonding between C1 and C2, between C1 and C4, between C6 and H11, and between C6 and H12; where we describe bonding

in the sense of Berlin's (34) binding and anti-binding regions in which, by the electrostatic theorem (35,36), the electron density acts to either pull nuclei together or separate them. Therefore, while the occupation of the 10B SO will decrease the bond order of the C1-C6 bond, it will concurrently lead to an increase in the bond order of the C-H methylene bonds and the C-C ring bonds, which is observed both visually and quantitatively through BB analysis. (The C1-C6 bond bundle size decreases through rotation, which is consistent with a loss of electrons, requiring the number of electrons in the C6-H and in the ring to increase. See Figure 2.3 and Figure 2.4.) BB analysis provides a sensitive probe of the interactions between atoms without sacrificing conceptual power.

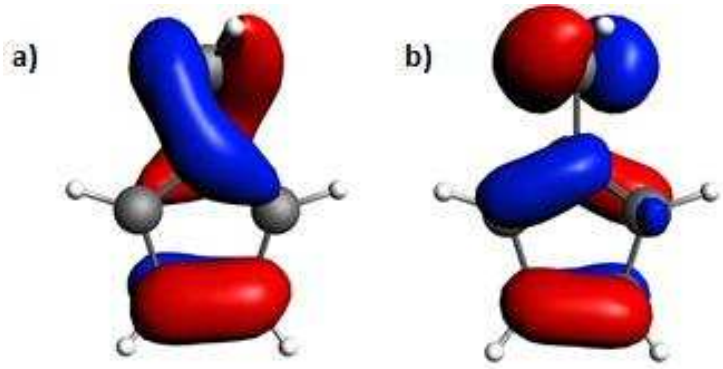

Figure 2.5: The near fermi energy SOs of the S_{63} coupled by the rotation (see Figure 2.2). The 12A SO (a) is π-bonding between C1 and C6 while the 10B SO (b) is π -antibonding between the same two atoms.

2.5. Conclusion

We demonstrate that bond bundles are an intuitive and accurate tool for visualizing the evolution of the entirety of the charge density associated with the rotation of the exo C-C double bond of fulvene. The BB approach provides a representation of rotation about a π-bond that is remarkably consistent with that from orbital approaches. The BB shows a continuous change

from open to closed that is consistent with a transformation from double to single bond character. The rate of closing appears to be related to the barrier to rotation, where the SU state—with a lower barrier to rotation—closes faster. In addition, the bond order, as determined from the integration of BB electron density, changes from 1.66 to 1.24 through the rotation, with the charge density lost from the C-C bond displaced to the methylene C-H bonds and the C ring structure. In all ways, the behavior of the BB transitioning from double to single bond complements conventional views of rotation of a π-bond, but is free from orbital representations and may be particularly useful for quantifying and rationalizing charge redistribution where orbital information is not available, such as from experimentally determined charge densities.

CHAPTER 3

FUTURE WORK AND CONCLUSIONS

In chapter 2, I have shown how bond bundles accurately represent the evolution of charge density during bond torsion in fulvene. The rate at which the BB closes in the SU state compared to the SR state is related to the barrier to rotation, where the SU state closes faster because it has a lower barrier to rotation. Moving forward, I will be using Gradient Bundle Analysis to evaluate how the movement of charge density in different molecules correlates to high and low barriers to rotation.

Bond bundles can be decomposed into smaller gradient bundles, which contain additional chemical property information. With an infinite number of ZFSs in $\rho(r)$, there are an infinite number of ways to partition a molecule into regions with well-defined properties. Gradient Bundle Analysis takes advantage of this partitioning by creating sub-regions from larger atomic basins or BBs. Gradient bundles are defined as bundles of gradient paths in the charge density in the volume bounded by ZFSs (24). Gradient Bundle Analysis can be used to find additional properties in the charge density.

For this study, a variety of substituted ethane and ethene molecules known to have electron withdrawing and donating properties will be used to observe how the charge density changes when the bond is rotated. I will begin by collecting experimentally and computationally calculated energy barriers to rotation for these molecules. ADF will be used to calculate the energy barriers of rotation using different functionals and integration schemes (11). These computational values will be compared to literature values to ensure a confident computation method for finding the energy barriers. After choosing a suitable functional and integration

scheme, we will calculate the barrier to rotation for all molecules. Their staggered and eclipsed geometries will be optimized using ADF and the charge densities will be analyzed using Tecplot (32). Steric hindrance is a factor in computing the barrier to rotation, therefore, trans-1,2-di-tert-butylethylene will be used to analyze the effect of steric hindrance in the gradient paths present in molecules with bulky substituents. I will be looking for how much drag there is in the gradient paths along the bond path of interest. Drag will be assessed by computing the mathematical torsion induced in the gradient bundles as a result from the rotation. I expect to see more torsion in the gradient paths that corresponds to a high barrier to rotation, and moreover, less torsion in gradient paths that have a low barrier to rotation. Less movement of the gradient paths in the charge density relates to a higher degree of malleability and takes less energy to distort the charge density. Understanding how the barrier to rotation relates to the charge density will improve how scientists analyze conformational isomers, for example proteins and enzymes in the human body and synthetic molecules in medicine.

REFERENCES CITED

1. Bader RFW. Atoms in Molecules, a Quantum Theory. Oxford, UK: Clarendon Press; 1990.

2. Geerlings P, De Proft F, Langenaeker W. Conceptual Density Functional Theory. Chem Rev. 2003;103(5):1793–874.

3. Bader RFW. Private Communication.

4. Shahbazian S, Zahedi M. Letter to the Editor: The concept of chemical bond - Some like it fuzzy but others concrete. Found Chem. 2007;9(1):85–95.

5. Poater J, Solà M, Bickelhaupt FM. A model of the chemical bond must be rooted in quantum mechanics, provide insight, and possess predictive power. Chem - A Eur J. 2006;12(10):2902–5.

6. Jones TE. Nucleophilic substitution: A charge density perspective. J Phys Chem A. 2012;116(16):4233–7.

7. Morgenstern A, Eberhart M. Bond dissociation energies from the topology of the charge density using gradient bundle analysis. Phys Scr. 2016;91(2):23012.

8. Morgenstern A, Morgenstern C, Miorelli J, Eberhart ME. The influence of zero-flux surface motion on chemical reactivity. Phys Chem Chem Phys. 2016;18:5638–46.

9. Miller JE. Relative Critical Sets in Rn and Applications to Image Analysis. University of Norther Carolina; 1998.

10. Smiley MF, Milnor J. Morse Theory. Vol. 71, The American Mathematical Monthly. 1964. 936 p.

11. ADF2016. SCM, Theoretical Chemistry, Vrije Universiteit, Amsterdam, The Netherlands, 2014.

12. Morgenstern A. Gradient Bundle Analysis: A Full Topological Approach to Chemical Bonding. Colorado School of Mines; 2016.

13. Popelier PLA. Characterization of a Dihydrogen Bond on the Basis of the Electron Density. J Phys Chem A. 1998;102(10):1873–8.

14. Matta CF, Boyd RJ. The Quantum Theory of Atoms in Molecules: From Solid State to DNA and Drug Design. Weinheim: Wiley-VCH; 2007. 567 p.

15. Jenkins S, Restrepo A, David J, Yin D, Kirk SR. Spanning QTAIM topology phase diagrams of water isomers W4, W5 and W6. Phys Chem Chem Phys. 2011;13(24):11644.

16. Runtz GR, Bader RFW, Messer RR. Definition of bond paths and bond directions in terms of the molecular charge distribution. Can J Chem. 1977;55(16):3040–5.

17. Anderson JSM, Ayers PW, Hernandez JIR. How ambiguous is the local kinetic energy? J Phys Chem A. 2010;114(33):8884–95.

18. Cohen L. Local kinetic energy in quantum mechanics. J Chem Phys. 1979;70(1979):788–9.

19. Ghosh SK, Parr RG. Density-determined orthonormal orbital approach to atomic energy functionals. J Chem Phys. 1985;82(1985):3307–15.

20. Pendás A, Costales A, Luaña V. Ions in crystals: the topology of the electron density in ionic materials. III. Geometry and ionic radii. J Phys Chem B. 1998;102(98):6937–48.

21. Eberhart M. A quantum description of the chemical bond. Philos Mag B. 2001;81(8):721–9.

22. Jones TE, Eberhart ME. The irreducible bundle: Further structure in the kinetic energy distribution. J Chem Phys. 2009;130(20).

23. Jones TE, Eberhart M. The Bond Bundle in Open Systems. Int J Quantum Chem. 2010;110:1500–5.

24. Morgenstern A, Wilson T, Miorelli J, Jones T, Eberhart ME. In search of an intrinsic chemical bond. Comput Theor Chem. 2015;1053:31–7.

25. Jones TE, Eberhart ME, Imlay S, MacKey C, Olson GB. Better alloys with quantum design. Phys Rev Lett. 2012;109(12):1–5.

26. Ayers PW, Jenkins S. An electron-preceding perspective on the deformation of materials. J Chem Phys. 2009;130(15).

27. Jenkins S, Blancafort L, Kirk SR, Bearpark MJ. The response of the electronic structure to electronic excitation and double bond torsion in fulvene: a combined QTAIM, stress tensor and MO perspective. Phys Chem Chem Phys. 2014;16(d):7115–26.

28. Bearpark MJ, Bernardi F, Olivucci M, Robb MA, Smith BR. Can fulvene S1 decay be controlled? A CASSCF study with MMVB dynamics. J Am Chem Soc. 1996;118(22):5254–60.

29. Bearpark MJ, Blancafort L, Paterson MJ. Mapping the intersection space of the ground and first excited states of fulvene. Mol Phys. 2006;104(5–7):1033–8.

30. Sicilia F, Bearpark MJ, Blancafort L, Robb MA. An analytical second-order description of the S 0 /S 1 intersection seam: Fulvene revisited. Theor Chem Acc. 2007;118(1):241–51.

31. SCM. ADF Manual. 2013;1–442.

32. Tecplot 2014. Available from: http://www.tecplot.com/

33. Bersuker I. The Jahn–Teller Effect. Cambridge: Cambridge University Press; 2006

34. Berlin T (University of M. Binding Regions in Diatomic Molecules. J Chem Phys. 1951;19(2):208–13.

35. Wang W, Hobza P. Application of Berlin's Theorem to Bond-Length Changes in Isolated Molecules and Red- and Blue-Shifting H-Bonded Clusters. Collect Czechoslov Chem Commun. 2008;73(6–7):862–72.

36. Wang X, Peng Z. Binding regions in polyatomic molecules. Int J Quantum Chem. 1993;47(5):393–404.

APPENDIX A

ADDITIONAL INFORMATION

This appendix presents tables referenced from Chapter 2. Tables of coordinates used in this study are available for geometries S_0, S_{63}, S_{90} in Table A.1, Table A.2, and Table A.3. Table A.4 gives coordinates for the S_{90} geometry optimized by ADF. Table A.5 compares the C1-C6 bond lengths for the geometries provided by Jenkin's *et al.* and the relaxed geometries calculated by ADF followed by a short summary sensitivity analysis conducted during this study is discussed. Table A.6 lists additional properties that were calculated for fulvene during the study. A table of Bader analysis calculated for S_0 and S_{90} geometries are presented in Table A.7. A compilation of bond lengths for each geometry of fulvene are located in Table A.8.

Table A.1: Coordinates for the S_0 geometry in atomic units (a.u.) referenced from the methods section.

S_0 Coordinates			
1 C	0.000000000000	0.000000000000	0.765607238500
2 C	0.000000000000	1.178185241000	-0.127825141900
3 C	0.000000000000	0.741603971800	-1.410840298000
4 C	0.000000000000	-1.178185241000	-0.127825141900
5 C	0.000000000000	-0.741603971800	-1.410840298000
6 C	0.000000000000	0.000000000000	2.114682322000
7 H	0.000000000000	2.202772336000	0.211656825100
8 H	0.000000000000	1.356535614000	-2.298638148000
9 H	0.000000000000	-2.202772336000	0.211656825100
10 H	0.000000000000	-1.356535614000	-2.298638148000
11 H	0.000000000000	0.924064131300	2.678105284000
12 H	0.000000000000	-0.924064131300	2.678105284000

Table A.2: Coordinates for the S_{63} geometry in atomic units (a.u.) referenced from the methods section.

S_{63} Coordinates			
1 C	0.000000000000	0.000000000000	0.740594957900
2 C	0.000000000000	1.131109007000	-0.099157047960
3 C	0.005298000048	0.685285001300	-1.491080053000
4 C	0.000000000000	-1.131109007000	-0.099157047960
5 C	-0.005298000048	-0.685285001300	-1.491080053000
6 C	0.000000000000	0.000000000000	2.222259964000
7 H	-0.020797000090	2.159732009000	0.228839953200
8 H	-0.002318000012	1.334500009000	-2.352894058000
9 H	0.020797000090	-2.159732009000	0.228839953200
10 H	0.002318000012	-1.334500009000	-2.352894058000
11 H	0.823921006000	0.427642001800	2.776911967000
12 H	-0.823921006000	-0.427642001800	2.776911967000

Table A.3: Coordinates for the S_{90} geometry in atomic units (a.u.) referenced from the methods section.

S_{90} Coordinates			
1 C	0.000000000000	0.000000000000	0.733190334700
2 C	0.000000000000	1.144880007000	-0.113064667000
3 C	0.000000000000	0.706689002400	-1.467670671000
4 C	0.000000000000	-1.144880007000	-0.113064667000
5 C	0.000000000000	-0.706689002400	-1.467670671000
6 C	0.000000000000	0.000000000000	2.211201345000
7 H	0.000000000000	2.170809011000	0.221992334500
8 H	0.000000000000	1.343811009000	-2.338434677000
9 H	0.000000000000	-2.170809011000	0.221992334500
10 H	0.000000000000	-1.343811009000	-2.338434677000
11 H	-0.927714004100	0.000000000000	2.767679348000
12 H	0.927714004100	0.000000000000	2.767679348000

Table A.4: Coordinates for the S_{90} optimized geometry using ADF. These coordinates are used to compare geometries between Jenkins.

	S_{90} Coordinates for ADF Optimized Geometry		
1 C	0.000000000000	0.000000000000	0.740516011400
2 C	0.000000000000	1.162619853000	-0.111150031300
3 C	0.000000000000	0.696734791800	-1.425236087000
4 C	0.000000000000	-1.162619853000	-0.111150031300
5 C	0.000000000000	-0.696734791800	-1.425236087000
6 C	0.000000000000	0.000000000000	2.111361931000
7 H	0.000000000000	2.177608047000	0.247339023800
8 H	0.000000000000	1.347570615000	-2.286859231000
9 H	0.000000000000	-2.177608047000	0.247339023800
10 H	0.000000000000	-1.347570615000	-2.286859231000
11 H	-0.918147915700	0.000000000000	2.713471264000
12 H	0.918147915700	0.000000000000	2.713471264000

Table A.5: Table shows the C1-C6 bond length (pm) for the 4 geometries shown in the main text. The first row shows the bond length of the coordinates given by Jenkins. The 30 degree bond length is a rigid rotation and was not found by relaxing the geometry. The second row shows the spin restricted bond length when the geometry was allowed to relax. The third and fourth rows show the spin unrestricted, singlet and triplet configurations respectively, relaxed geometries optimized using ADF.

Degree Rotation	0 Deg C1-C6 (pm)	30 Deg C1-C6 (pm)	63 Deg C1-C6 (pm)	90 Deg C1-C6 (pm)
Coord. Provided by Jenkins	135	134	148	148
SR ADF Geometry	133	134	137	137
SU (singlet) ADF Geometry	142	144	146	145
SU (triplet) ADF Geometry	139	141	146	145

Sensitivity Analysis

During this study, we assessed the sensitivity of the bond bundle to changes in atomic coordinates, singlet versus triplet excited states, and functional. First we compared the atomic coordinates for S_{90} provided by Jenkins with coordinates the SU triplet geometry optimized using ADF. The bond lengths can be found in table A3. The bond lengths are 148 and 145 pm respectively. After examining both charge densities using Tecplot, the bond bundles are visually indistinguishable and the valence electron counts differ by 0.1 electrons, 3.46 and 3.56 valence electrons respectively. The qualitative arguments in this paper are not effect by changes in atomic coordinates.

Table A.6: Properties for fulvene at all incremented angles that were calculated during the study. The first column on the left shows the calculated SR valence electron count in the bond bundle and second column presents the SR bond bundle volume. The SU triplet and singlet valence electron counts and volumes are shown in the next 4 columns. Finally, the last 2 columns are the right show the C6-H11 valence electron count and bond bundle volume for the S_0 and S_{90} geometries.

Degree	SR Electron Count	SR BB Volume (a.u.)	SU (triplet) Electron Count	SU (triplet) BB Volume (a.u.)	SU (singlet) Electron Count	SU (singlet) BB Volume (a.u.)	SU C6-H11 Electron Count	SU C6-H11 BB Volume (a.u.)
10	3.391	74.650	-	-	-	-	-	-
20	3.287	70.760	-	-	-	-	-	-
30	3.211	68.330	3.184	48.840	-	-	-	-
40	3.032	62.850	-	-	-	-	-	-
50	2.847	57.950	-	-	-	-	-	-
63	2.357	48.610	3.109	48.509	2.370	36.810	-	-
70	2.676	53.410	2.748	44.578	-	-	-	-
80	2.781	55.270	2.707	44.120	-	-	-	-
90	3.640	66.678	2.468	44.900	2.256	36.076	2.299	72.46

Table A.7: Bader analysis properties calculated by ADF referenced in the results section. For S_0 and S_{90} geometries the density, net charge, spin density, and Laplacian were calculated for each atom in fulvene. The last column on the right shows the change in net charge when you move from S_0 to S_{90} giving a better idea of the electron movement throughout the molecule during bond torsion.

	S_0 Bader Analysis				S_{90} Bader Analysis				
Atom	Density	Net Charge	Spin Density	Laplacian	Density	Net Charge	Spin Density	Laplacian	Δ Net Charge
C1	5.9987	0.0013	0	-1.17E-02	6.0101	-0.0101	0.4936	-1.42E-04	-0.4937
C2	6.0418	-0.0418	0	2.30E-04	6.0418	-0.0418	-0.0135	-1.69E-03	0.0118
C3	6.0300	-0.0300	0	-6.26E-03	6.0143	-0.0143	0.2775	-5.80E-03	-0.2833
C4	6.0418	-0.0418	0	2.30E-04	6.0418	-0.0418	-0.0135	-1.69E-03	0.0118
C5	6.0300	-0.0300	0	-6.26E-03	6.0143	-0.0143	0.2775	-5.80E-03	-0.2833
C6	6.0006	-0.0006	0	-6.04E-04	6.0612	-0.0612	0.8921	-7.92E-03	-0.9000
H7	0.9759	0.0241	0	2.45E-03	0.9798	0.0202	-0.0008	5.79E-04	0.0014
H8	0.9726	0.0274	0	4.91E-03	0.9712	0.0288	0.0047	4.95E-03	0.0002
H9	0.9759	0.0241	0	2.45E-03	0.9798	0.0202	-0.0008	5.79E-04	0.0014
H10	0.9726	0.0274	0	4.91E-03	0.9712	0.0288	0.0047	4.95E-03	0.0002
H11	0.9800	0.0200	0	4.52E-03	0.9572	0.0428	0.0393	5.57E-03	-0.0337
H12	0.9800	0.0200	0	4.52E-03	0.9572	0.0428	0.0393	5.57E-03	-0.0337

Total	41.999	0.0001	0.0000	-0.0006	41.999	0.0001	2.0001	-0.0008	0

Table A.8: The bond lengths (in pm) for each geometry are shown.

Bond lengths (pm)										
Degree	0	10	20	30	40	50	63	70	80	90
C1-C6	135	134	134	134	135	135	148	138	139	148
C2-C1	147.9	147.1	147.1	147.1	147	146.8	140.9	146.3	145.8	142.4
C3 - C2	135.5	134.5	134.5	134.6	134.7	134.9	146.2	135.6	136	142.4
C4 - C1	147.9	147.1	147.1	147.1	147	146.8	140.9	146.3	145.8	142.4
C5-C4	135.5	134.5	134.5	134.6	134.7	134.9	146.2	135.6	136	142.4
C5-C3	148.3	147.2	147.1	147	146.8	146.5	137.1	145.8	145.4	141.3
H7 -C2	108	108	108	108	108	108	108	108	108	108
H8 -C3	108	108	108	108	108	108	108	108	108	108
H9 - C4	108	108	108	108	108	108	108	108	108	108
H10 -C5	108	108	108	108	108	108	108	108	108	108
H11-C6	108	108	108	108	108	108	108	109	109	108
H12-C6	108	108	108	108	108	108	108	109	109	108

APPENDIX B

PERMISSIONS

This appendix provides permissions from co-authors of submitted material presented in this thesis.

B.1 Author Permissions

Tim Wilson (Chapter 2), twilson@mines.edu
I, Timothy Robert Wilson, do hereby grant you permission to use the article, “Visualizing the evolution of charge density in fulvene bond torsion: a bond bundle case study,” of which I am an author, in your master’s thesis.

Sincerely,
Tim

Amanda Morgenstern (Chapter 2), amorgens@mines.edu
I give you permission to reproduce our paper, "Visualizing the Evolution of Charge Density in Fulvene Bond Torsion: A Bond Bundle Case Study" in your thesis.

Best,
Amanda